The Practical Use of Phase Diagrams

D.R. Gaskell
School of Materials Engineering
Purdue University
1289 Materials & Electrical Engineering Bldg.
West Lafayette, IN 47907-1289

(Submitted March 25, 1993)

Phase diagrams are graphical representations of the states of equilibrium available to materials systems and the influence on the equilibrium states of changes in composition, temperature, and pressure. They are governed by the phase rule, which relates the number of degrees of freedom that an equilibrium has to the number of components and the number of phases occurring in the system. Phase equilibria in unary, binary, ternary, and quaternary systems are discussed, and phase and stability diagrams are applied to an understanding of vacuum sublimation, the removal of copper from liquid lead, the galvannealing of steel, tool steels, the production of Ti-B-C composites, stainless steels, the production of SiC and Si_4N_3, Al_2O_3-SiC composites, and processing of the superconducting oxide $YBa_2Cu_3O_{7-x}$.

Introduction

Phase diagrams are graphical representations of the equilibrium states occurring in materials systems, and the degree of complexity of a phase diagram is determined primarily by the number of components that the system contains, where components are chemical species of fixed composition. The simplest components are chemical elements and stoichiometric compounds, and systems are categorized by the number of components that they contain, e.g. one-component (unary) systems, two-component (binary) systems, three-component (ternary) systems, four-component (quaternary) systems, etc.

This paper was presented as a tutorial luncheon lecture in Denver at the 122nd Annual TMS Meeting.

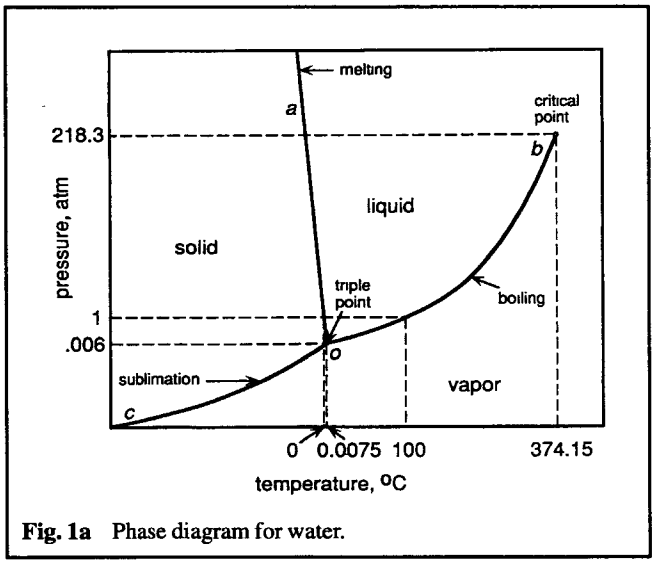

Fig. 1a Phase diagram for water.

Phase equilibria are governed by a simple, but powerful, rule called the Gibbs phase rule, which states that:

$$P + F = C + 2$$

in which P is the number of phases occurring, F is the number of degrees of freedom that the equilibrium has, and C is the number of components in the system. The number of degrees of freedom is the number of variables available to the system that can be independently varied without upsetting the equilibrium.

Unary Systems

The phase diagram for a unary system (a system of fixed composition) is a two-dimensional representation of the depend-

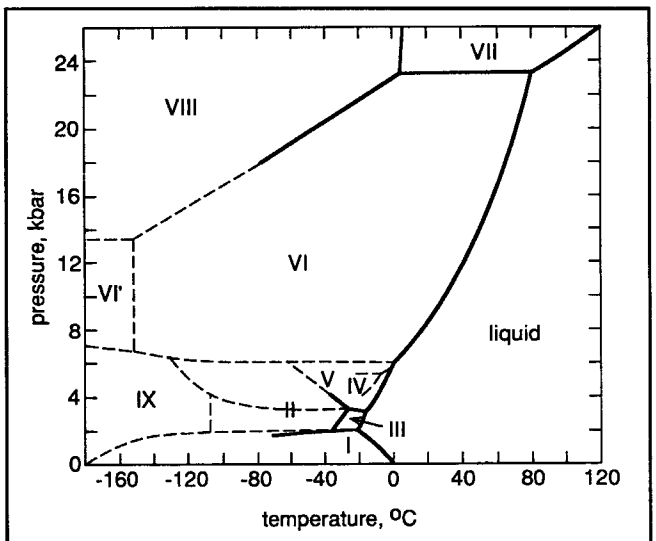

Fig. 1b Phase diagram for water for a wider range of temperature and pressure.

ence of the equilibrium states of the system on temperature and pressure, which are the only two variables available to the system. The phase diagram for water, shown in Fig. 1a, shows the stability fields of ice, liquid water, and water vapor in pressure-temperature space. There are two degrees of freedom in each of these single-phase fields, and hence the temperature and pressure can be varied independently without causing a change in the state of the system. The fields meet at lines that represent states in which two phases coexist. For example, solid and liquid water coexist in states along the *ao* line, and thus *ao* represents the influence of pressure on the melting temperature of ice. Similarly the *bo* line represents the variation with temperature of the saturated vapor pressure of liquid water or, correspondingly, the influence of pressure on the dew point of water vapor or the boiling temperature of liquid water. The *co* line is the variation with temperature of the saturated vapor pressure of ice. Two-phase equilibria have only one degree of freedom; i.e. only the temperature or the pressure can be varied independently. The three two-phase equilibrium lines meet at an invariant point called the triple point, which is the unique temperature and pressure at which the three phases are in equilibrium with each other. This three-phase equilibrium has no degrees of freedom, and hence, three is the maximum number of phases that can coexist in equilibrium in a unary system. The boiling curve ends at the critical point, *b*, in which state the molar volumes of the vapor phase and the liquid phase are equal, and the latent heat of boiling is zero. At pressures and temperatures higher than those of the critical point, water exists as a supercritical fluid. The transformation from a lower temperature phase (ice) to a higher temperature phase (liquid water) increases the enthalpy and the entropy of the system, and the transformation from a lower pressure phase (water vapor) to a higher pressure phase (liquid water) is accompanied by a decrease in the volume of the system. The normal melting and boiling temperatures of water, i.e. the values at a pressure of 1 atmosphere, are the reference points on the Celsius temperature scale.

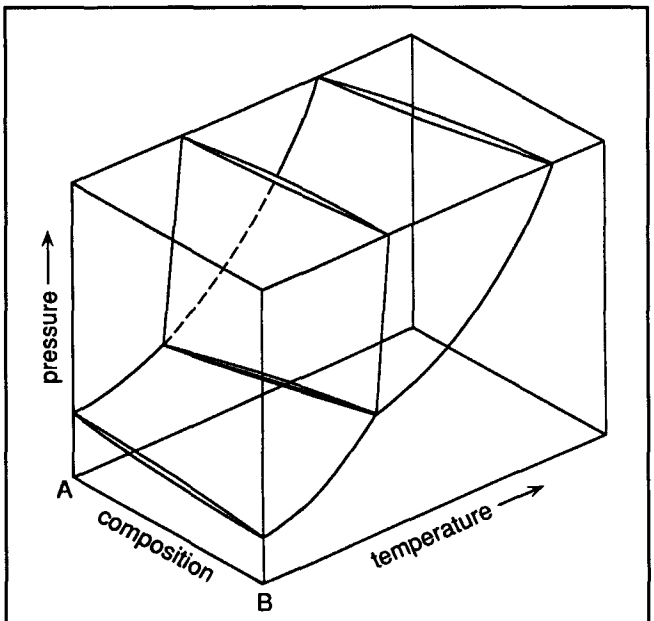

Fig. 2 Binary system phase diagram.

The phase diagram for water is shown for a wider range of temperature and pressure in Fig. 1b. Water has ten allotropic forms, and the pressure-induced decrease in the melting temperature of ice I stops at –22 °C, which is the temperature of the ice I-ice III-liquid triple point.

Binary Systems

The requirement of a composition axis in a binary phase diagram produces a three-dimensional phase diagram, such as is shown in Fig. 2. However, it is usual, and normally sufficient, to consider a binary phase diagram as an isobaric section of the three-dimensional diagram. The specification of the pressure at which the section is drawn uses one of the degrees of freedom available to phase equilibria in the system. The upper surface of Fig. 2 is reproduced as a two-dimensional composition-temperature diagram in Fig. 3. At a high enough temperature, the system exists as a vapor. When cooled at constant total pressure, the state of the composition *X* reaches the saturation point *a* at which point the liquid of composition *b* condenses. The *ab* line, which is drawn between the compositions of the equilibrated phases, is called a tie-line. Further decrease in temperature causes the composition of the equilibrium vapor to move down the *ac* line, and the composition of the equilibrium liquid moves down the *bd* line. At any temperature, the relative proportions of the two phases are given by application of the lever rule. On further cooling, the liquid reaches the state *e* at which point solidification begins. The solidification process is analogous with the condensation process, with the composition of the equilibrium liquid mov-

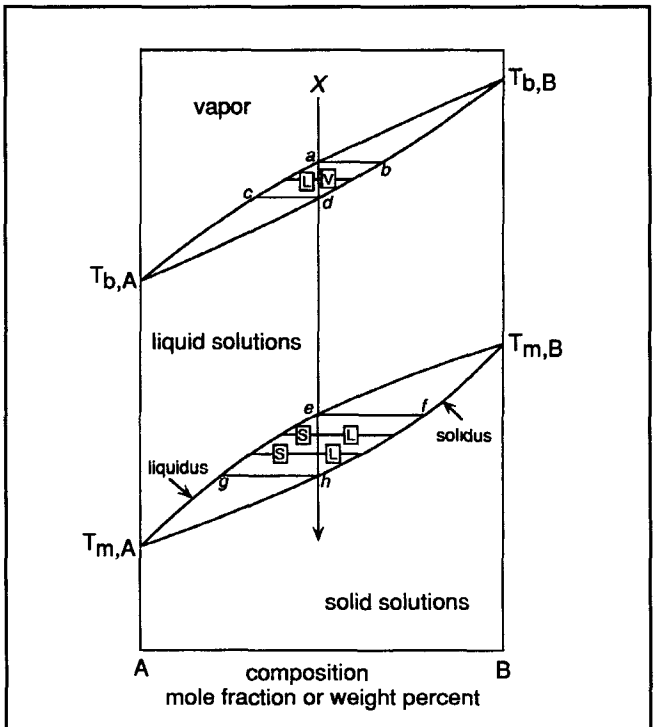

Fig. 3 Isobaric section of a binary phase diagram.

ing down the liquidus line from *e* to *g*, and the composition of the equilibrium solid moving down the solidus line from *f* to *h*. In binary systems, the transformation of one phase to another occurs over a range of temperature; whereas in unary systems, it occurs at a fixed temperature. The phase diagram for the Cu-Ni system is shown in Fig. 4. Copper and nickel have the same crystal structure and similar atomic radii, valences, and electronegativities, and hence they form a complete range of solid solutions.

Eutectic behavior in a binary system is shown in Fig. 5a, in which the isobaric section is drawn at a pressure higher than the triple point pressures of both components and is also shown in Fig. 5b in which the isobaric section is drawn at a pressure higher than the triple-point pressure of component *A* but lower than the triple-point pressure of component *B*. The maximum number of phases that can coexist in equilibrium in a binary system at an arbitrary pressure is three. Thus a eutectic equilibrium exists at a fixed temperature between two solid solutions of fixed composition and a liquid solution of fixed composition, which lies between those of the solids. Eutectic behavior usually occurs when either the atomic radii of the components and/or the crystal structures of the components are dissimilar. Figure 5a shows one three-phase eutectic equilibrium, and Fig. 5b shows a second three-phase vapor-liquid-β equilibrium.

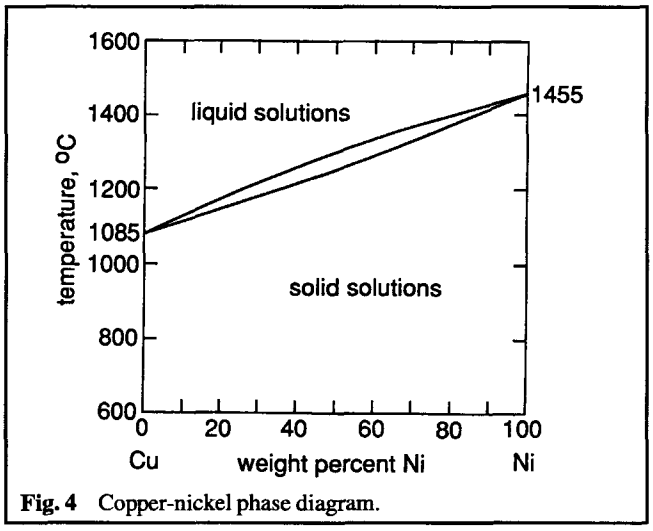

Fig. 4 Copper-nickel phase diagram.

The influence of pressure on the phase equilibria occurring in the Cd-Zn system is shown in Fig. 6.[1] At a pressure of 1 atm, the phase diagram is similar to that shown in Fig. 5a. The normal boiling temperatures of Cd and Zn are, respectively, 765 and 908 °C, and at 266 °C, a eutectic equilibrium occurs between solid solutions containing mole fractions of Zn of 0.044 and 0.987 and a eutectic liquid of $X_{Zn} = 0.266$. Decreasing the pressure to 10^{-3} atm has very little influence on the solid-liquid equilibria but significantly decreases the boiling temperatures. Further decrease in the pressure produces a phase diagram similar to that shown in Fig. 5b. At a pressure of 10^{-4} atm, which is lower than the triple-point pressures of both Cd and Zn, the liquid phase field is restricted to the center of the diagram. At 10^{-4} atm, the phase diagram contains 3 three-phase equilibria shown schematically in Fig. 6d. Further decrease in pressure causes a decrease in the temperature of the vapor-liquid-β equilibrium, and a decrease in the temperature of the vapor-α-liquid equilibrium and, eventually, the temperatures of the 3 three-phase equilibria coincide at a unique pressure to produce a four-phase equilibrium. This four-phase equilibrium has no degrees of freedom, and hence, like the triple point in a unary system, occurs at a unique pressure and a unique temperature. At pressures less than this unique pressure, the four-phase equilibrium is destroyed, and the liquid phase disappears.

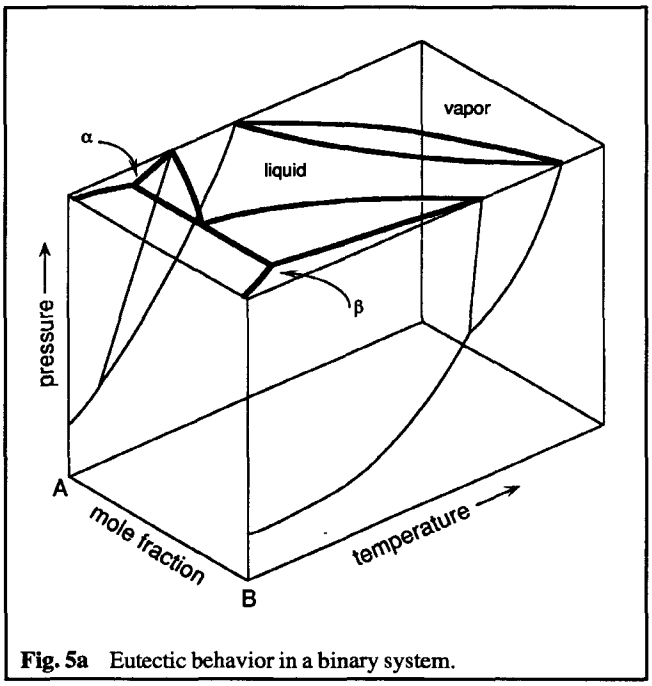

Fig. 5a Eutectic behavior in a binary system.

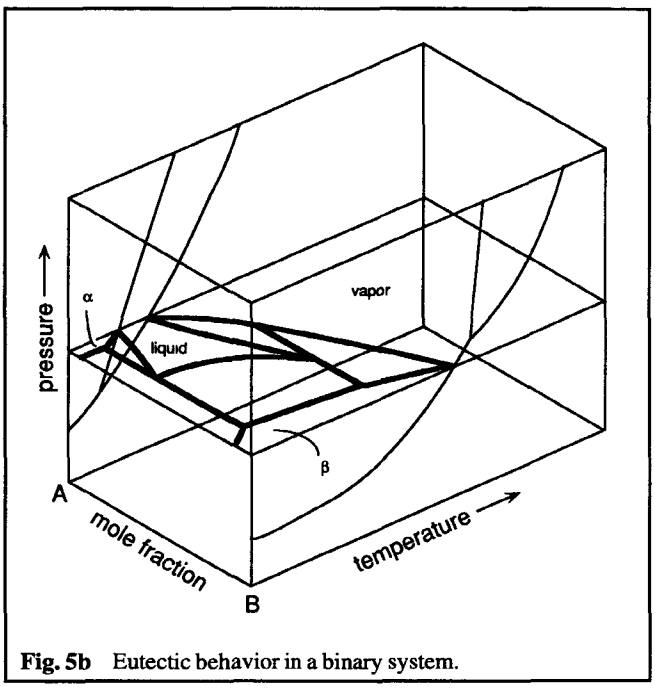

Fig. 5b Eutectic behavior in a binary system.

Consider 1 mol of the composition $X_{Zn} = 0.9$ at 1 atm pressure and 315 °C. Figure 6a shows that this system exists as 0.796 mol of β of $X_{Zn} = 0.99$ and 0.204 mol of liquid of $X_{Zn} = 0.55$. Figure 6c shows that decreasing the pressure of this system to 10^{-4} atm transforms it to 0.905 mol of β of $X_{Zn} = 0.99$ and 0.095 mol of vapor phase of $X_{Zn} = 0.045$. The vapor-solid equilibrium facilitates removal of Cd from the solid alloy by vacuum sublimation. Figure 6b shows that increasing the pressure of the Cd-rich vapor to 10^{-3} atm causes condensation to form a Cd-rich liquid at 315 °C. The influence of pressure on the phase equilibria occurring at 302 °C is shown in Fig. 7, which shows that, at this temperature, the liquid phase does not exist at pressures less than 7×10^{-5} atm.[1]

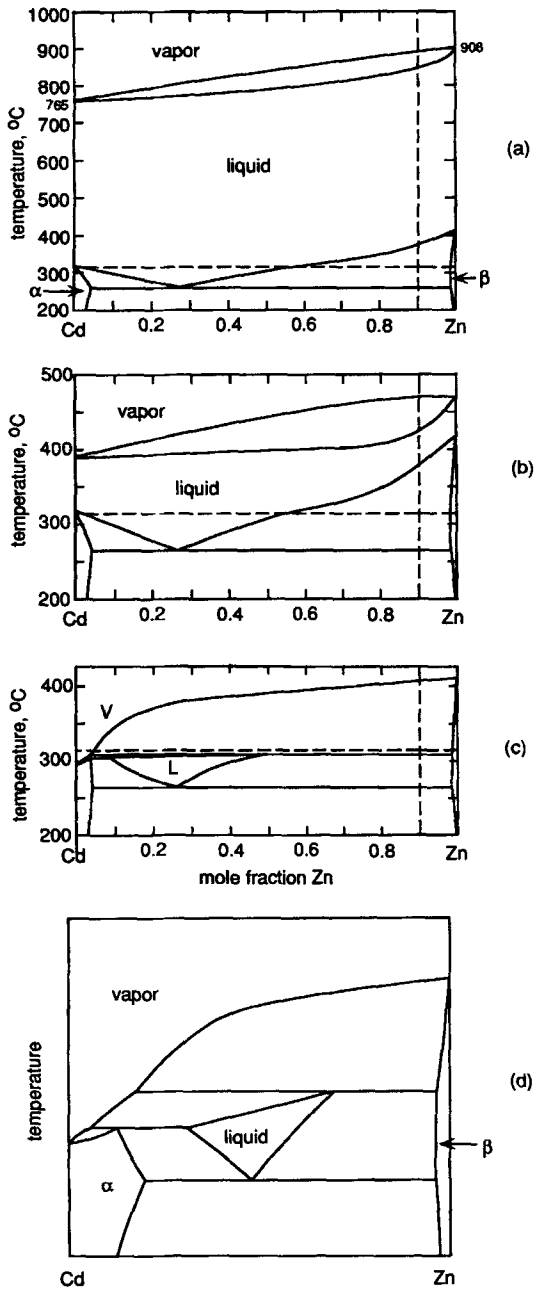

Fig. 6 Influence of pressure on phase equilibria in the Cd-Zn system. **(a)** $P_T = 1$ atm. **(b)** $P_T = 10^{-3}$ atm. **(c)** $P_T = 10^{-4}$ atm. **(d)** Schematic representation at $P = 10^{-4}$ atm.

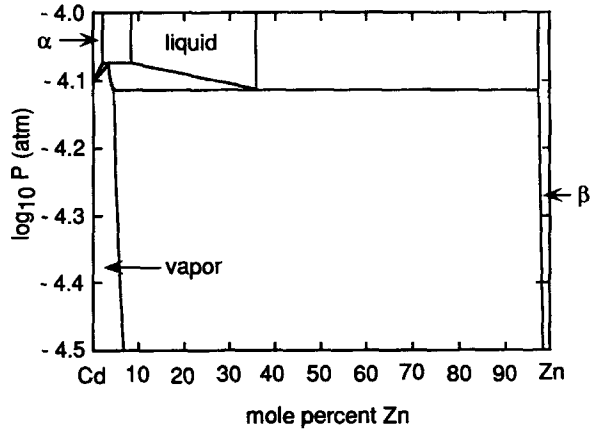

Fig. 7 Influence of pressure on phase equilibria in the Cd-Zn system at 302 °C.

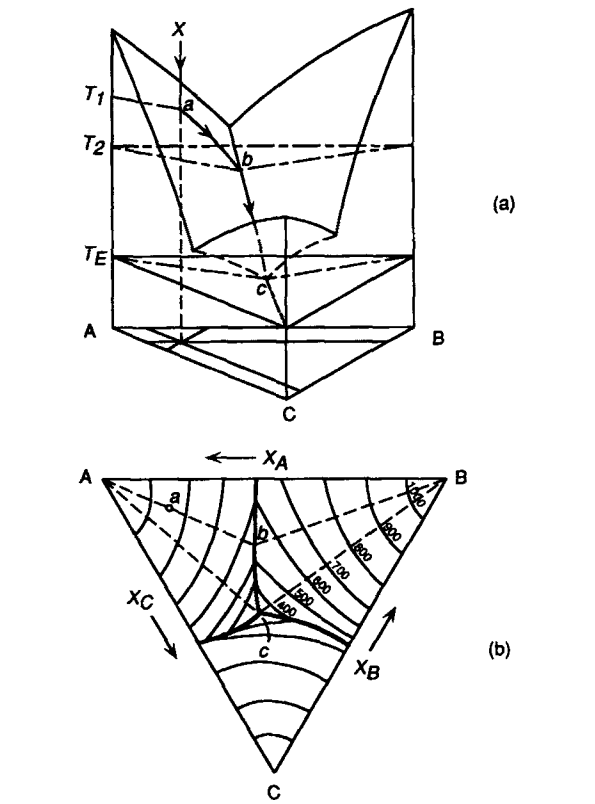

Fig. 8 Simple ternary phase diagram.

Ternary Systems

A three-component (ternary) system requires two composition axes, and hence the complete phase diagram requires four axes. Consequently, a ternary phase diagram is drawn at a constant pressure in three dimensions. The composition of a ternary system is most conveniently represented in a Gibbs triangle, shown in Fig. 8b, and a perspective of the three-dimensional diagram is shown in Fig. 8a, in which the temperature is plotted on the vertical axis. The system shown in Fig. 8 is one in which the three constituent binary systems are simple eutectics that exhibit negligible solid solubility. Phase equilibria in a ternary system have one more degree of freedom than the corresponding equilibria in a binary system. Thus areas such as liquid, α, and β in a binary phase diagram (shown in Fig. 6) become volumes in a ternary phase diagram. Liquidus and solidus lines in a binary become surfaces in a ternary. The point that represents a doubly saturated liquid in a binary becomes a line in a ternary. Consider the equilibrium freezing of the composition *X* in Fig. 8. At a high enough temperature, the system occurs in the liquid state volume, and on cooling, the state reaches the liquidus surface of *A* at the temperature T_1 in Fig. 8a, which from Fig. 8b is ~850 °C. At T_1, primary crystallization of pure *A* begins, and with continued cooling, the composition of the liquid moves down the liquidus surface from *a* towards *b*. At the temperature T_2 (500 °C in Fig. 8b), the liquid reaches the composition *b*, at which point it is saturated with solid *B*, and this marks the end of primary crystallization of *A*, which occurred over the range of temperature T_1 to T_2. On further cooling, secondary crystallization of *A* and *B* occurs, and the composition of the doubly saturated melt moves down the doubly saturated line from *b* towards *c*. At the temperature T_E, the liquid reaches the composition *c* in which state it is saturated with *C*, and a four-phase *A*-*B*-*C*-liquid equilibrium occurs. At constant pressure, a four-phase equilibrium in a ternary system has no degrees of freedom, and hence the maximum number of phases that can coexist in equilibrium in a ternary system is four. This equilibrium occurs at the unique ternary eutectic temperature T_E. Further withdrawal of heat from the system causes isothermal ternary eutectic decomposition of the liquid to form solid *A*, *B*, and *C*, and when this de-

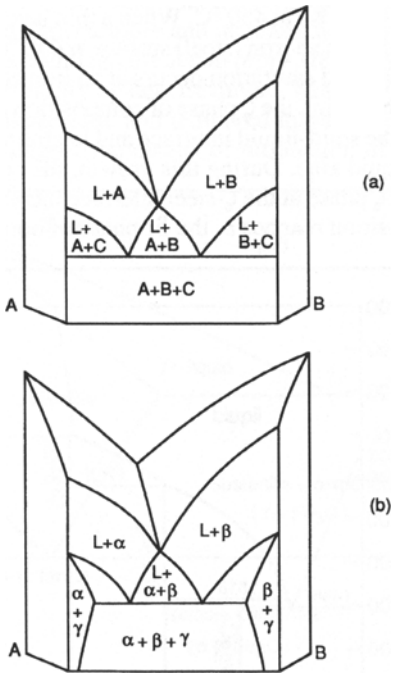

Fig. 9 Vertical sections of the ternary phase diagram shown in Fig. 8. **(a)** A system showing negligible solid solubility. **(b)** A system showing limited solid solubility.

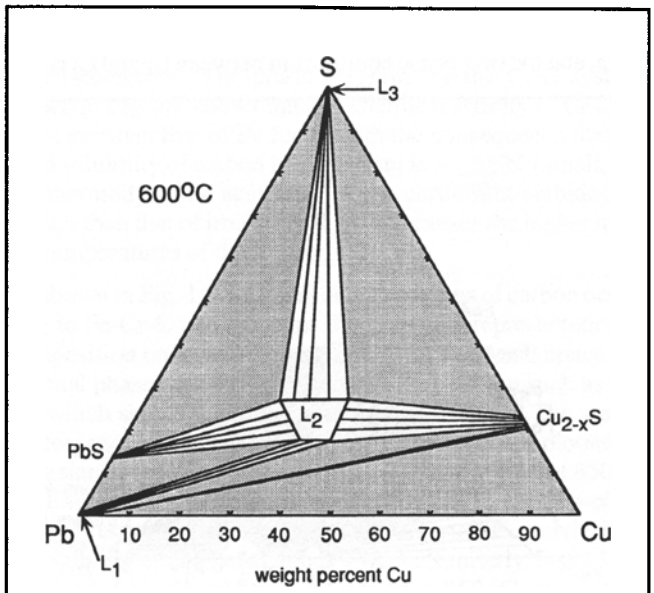

Fig. 10 Pb-Cu-S phase equilibria at 600 °C.

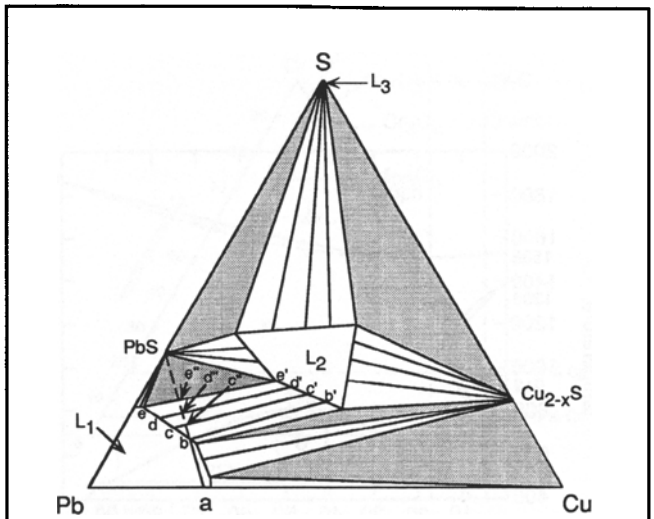

Fig. 11 Schematic representation of the phase equilibria shown in Fig. 10.

composition is complete, the system contains primary, secondary, and tertiary *A*, secondary and tertiary *B*, and tertiary *C*. A vertical section of the phase diagram is shown in Fig. 9a, and a vertical section of a ternary eutectic system showing limited solid solubility is shown in Fig. 9b.

The removal of copper from liquid lead can be understood from examination of the phase diagram for the Pb-Cu-S system, the 600 °C isothermal section of which is shown in Fig. 10.[2] The system contains stoichiometric PbS, nonstoichiometric $Cu_{2-x}S$, and three liquids: L_1, which is a dilute solution of copper and sulfur in liquid lead, L_2, a liquid lead copper sulfide, and L_3, liquid sulfur. Five three-phase equilibria occur: PbS-L_2-L_3, L_2-L_3-$Cu_{2-x}S$, L_1-$Cu_{2-x}S$-Cu, L_1-L_2-$Cu_{2-x}S$, and L_1-PbS-L_2. These three-phase equilibria, which are shown as shaded triangles in Fig. 10 and subsequent isothermal sections of ternary phase diagrams, are separated by two-phase equilibria, and the two-phase equilibrium between L_1 and L_2 is of interest. Consider L_1 of composition *a* shown in Fig. 11, which is a schematic reproduction of Fig. 10. The addition of PbS to melt *a* causes the composition to move across the L_1 phase field along the straight line between *a* and PbS. Saturation of the melt occurs when its composition reaches *b*, at which point it is in equilibrium with liquid L_2 of composition *b'*. Further addition of PbS causes the formation of L_2 as a second liquid phase. The overall composition of the system progresses along the path *c''-d''* to *e''* through the two-phase field with the composition of the L_1 moving along the saturation line *c-d* to *e* and the composition of L_2 moving along the saturation line *c'-d'* to *e'*. At *e''*, the system is saturated with PbS, and any further addition of PbS simply moves the overall composition of the system into the PbS-*e-e'* phase triangle without changing the compositions of the three phases occurring. The shape of the line of saturation between *b* and *e* is such that, as the second liquid L_2 separates from the metallic lead phase, the copper concentration in the latter decreases. At *e''*, which is the endpoint of the decoppering process, the two liquid phases occur in the ratio $L_1/L_2 = e''e'/ee''$.

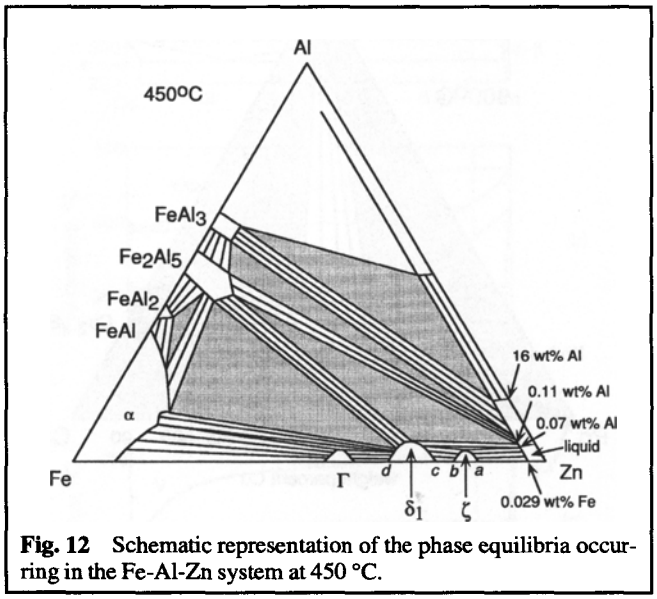

Fig. 12 Schematic representation of the phase equilibria occurring in the Fe-Al-Zn system at 450 °C.

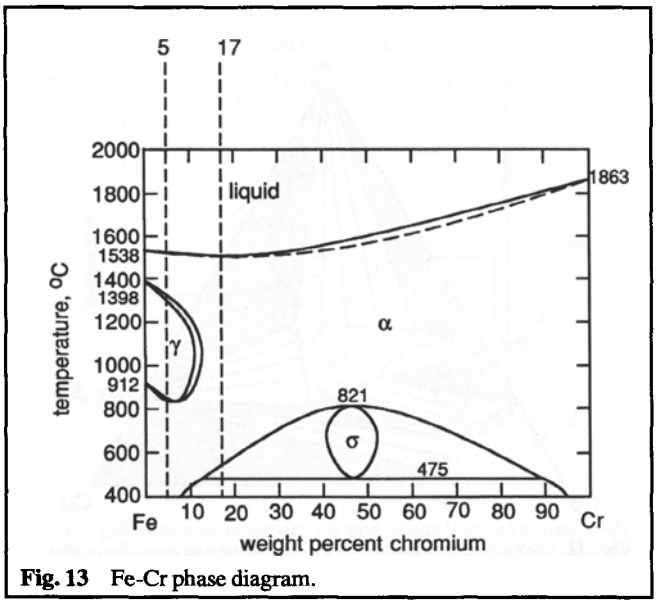

Fig. 13 Fe-Cr phase diagram.

Control of the kinetics of galvannealing of steel can be understood by examination of phase equilibria in the Fe-Al-Zn system. A schematic representation of the equilibria in this system at 450 °C is shown in Fig. 12,[3] in which the eight white areas are single-phase fields, and the seven shaded triangles are three-phase equilibria. The Fe-Al binary system contains four intermetallic phases, three of which can contain significant concentrations of zinc, and the binary system Fe-Zn contains three intermetallic phases, all of which are capable of dissolving aluminum. The liquidus composition in binary Zn-Al occurs at 16 wt.% Al, and Fe has a very small solubility in the liquid Zn-Al alloys at 450 °C. When a thin layer of pure liquid zinc is placed on an iron (steel) surface at 450 °C, Fe dissolves in the liquid, and saturation occurs at an iron content of 0.029 wt.%. At this point, the ζ phase of composition *a* in Fig. 12 nucleates at the solid-liquid interface and begins to grow into the layer of liquid zinc. During this growth, the concentration of iron in the ζ phase at the ζ-steel interface increases, and when the composition reaches *b*, the δ_1 phase of composition *c* nu-

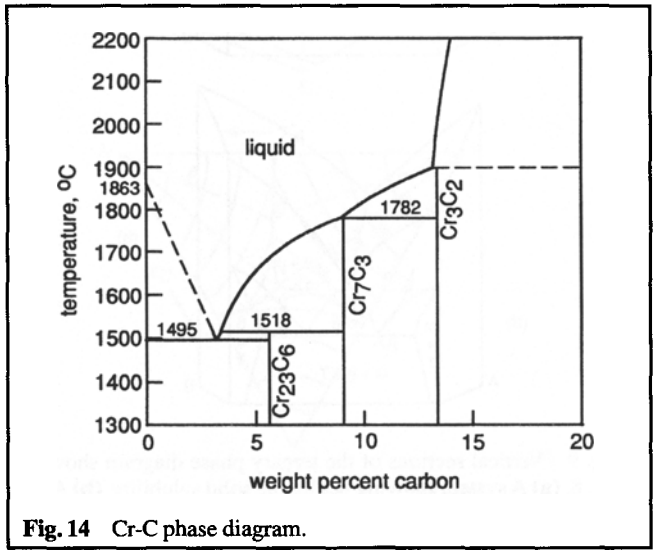

Fig. 14 Cr-C phase diagram.

cleates and begins to grow into the ζ phase. Given enough time, the composition of the δ_1 phase in contact with the steel moves to the point *d*, and the Γ phase nucleates and begins to grow into the δ_1. Thus, during the galvannealing of steel, all three intermetallics can be present in the galvannealed layer. Also, when the advancing layer of ζ phase consumes the liquid zinc, it in turn is then consumed by the advancing δ_1 phase. The reactions that occur during galvannealing are extremely rapid and over-galvannealing can occur during the time required to run the zinc-coated steel strip through the galvannealing furnace. Consequently, the galvannealing reactions are inhibited by adding Al to the liquid zinc. Figure 12 shows that the liquid zinc phase, which is doubly saturated with Fe_2Al_5 and δ_1, contains 0.11 wt.% Al, and the liquid zinc phase, which is doubly saturated with δ_1 and ζ, contains 0.07 wt.% Al. Thus, if the zinc used for galvannealing contains slightly more than 0.11 wt.% Al, the phase that first nucleates on the steel, as a result of dissolution of Fe in the melt, is Fe_2Al_5. Growth of this layer causes a decrease in the Al content of the liquid, and when the weight percentage of Al has been decreased to 0.07, the melt is in equilibrium with both δ_1 and Fe_2Al_5. Further decrease in the aluminum content of the melt moves the system into the liquid-δ_1 two-phase region, which causes the nucleation and growth of δ_1 on the steel and the dissolution of Fe_2Al_5. The rate of growth of the initial Fe_2Al_5 layer is significantly lower than the rate of growth of the δ_1 layer, and hence the initial time period during which the Fe_2Al_5 grows can be considered to be an incubation period, the length of which is determined by the initial concentration of Al in the liquid zinc.

Tool steels are high-carbon iron-based alloys containing combinations of Cr, W, Mo, and V as alloying agents. The alloying elements form hard carbides and increase the hardenability of the alloy. Thus, although the actual properties of tool steels are determined primarily by heat treatment, which produces nonequilibrium martensitic and tempered martensitic structures, an understanding of the means of production of the desired properties requires knowledge of the equilibrium phase relationships, which occur in the annealed alloy prior to quenching and tempering. Phase equilibrium in the Fe-Cr-C ternary system will be considered. The phase diagram for the Fe-Cr binary system is shown in Fig. 13. Iron is allotropic in that, in the solid state at temperatures below 912 °C and above 1398 °C it exists as the α phase with a bcc crystal structure, and between 912 and 1398 °C, it exists as the γ phase with an fcc structure. Chromium has the bcc structure, and hence when alloyed with Fe, stabilizes the α phase and produces the γ-loop shown in Fig. 13. In contrast, carbon stabilizes the γ phase, and when added to iron, produces the well-known Fe-Fe_3C phase diagram shown in Fig. 15, in which the solid solution containing carbon in fcc iron is called austenite, and the solid solution containing carbon in bcc iron is called ferrite. The extent of solid solution of carbon in solid iron at temperatures below the eutectic is determined by the precipitation of Fe_3C, which is called cementite. The phase diagram for the Cr-C system, shown in Fig. 14, shows that the chemical affinity of Cr for C is greater than that of Fe for C, with the consequence that the solid solubility of carbon in chromium is negligibly small, and the thermodynamic stabilities of the chromium carbides are greater than that of iron carbide, which causes the higher melting temperatures of the former.

As shown in Fig. 16, the small concentrations of carbon occurring in Fe-Cr-C alloys makes the graphical representation of composition on a Gibbs triangle inconvenient, and hence isothermal phase equilibria are shown on a diagram such as Fig. 17, which shows the phase equilibria at 850 °C.[4] The weight percentages of the alloying agents Cr and C are plotted on cartesian coordinates. Figures 15 and 17b show that, at 850 °C, the limit of solubility of C in ferrite is ~0.015, the two-phase field of ferrite + austenite extends to 0.2 wt.% C, and the limit of solubility of C in austenite is 1 wt.%. Similarly, Fig. 13 and 17b show how the addition of Cr to Fe at 850 °C creates the γ loop with a very narrow α+γ two-phase region near 5 wt.% Cr and a wider two-phase region extending from 8.5 to 10.5 wt.%

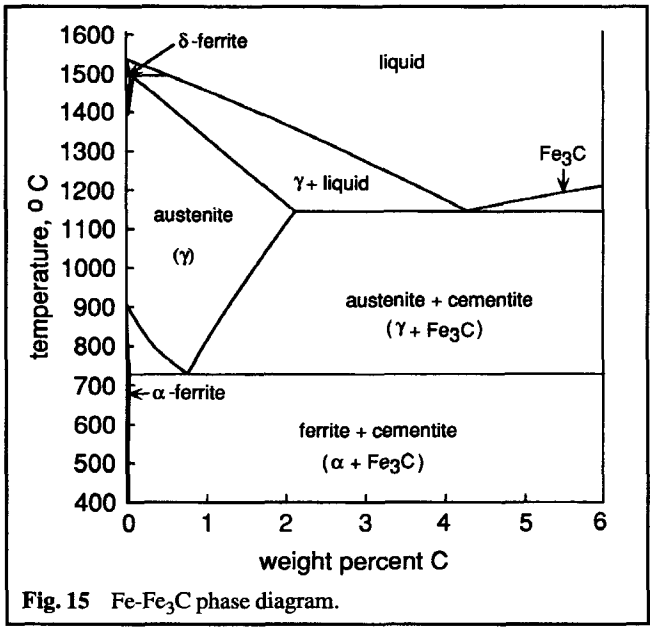

Fig. 15 Fe-Fe_3C phase diagram.

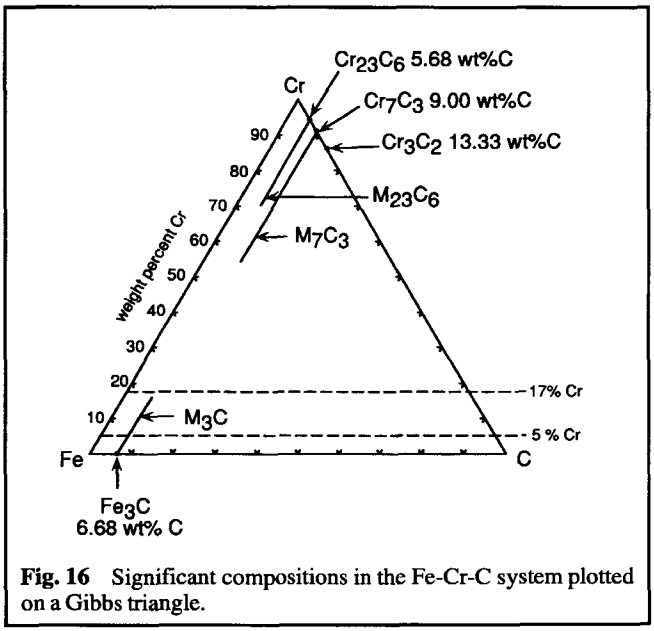

Fig. 16 Significant compositions in the Fe-Cr-C system plotted on a Gibbs triangle.

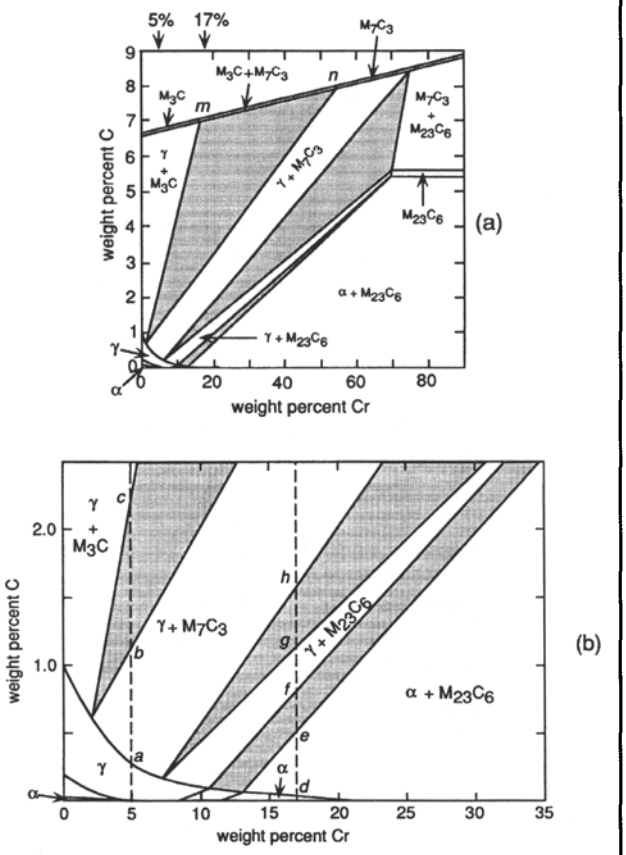

Fig. 17 Fe-Cr-C phase equilibria at 850 °C.

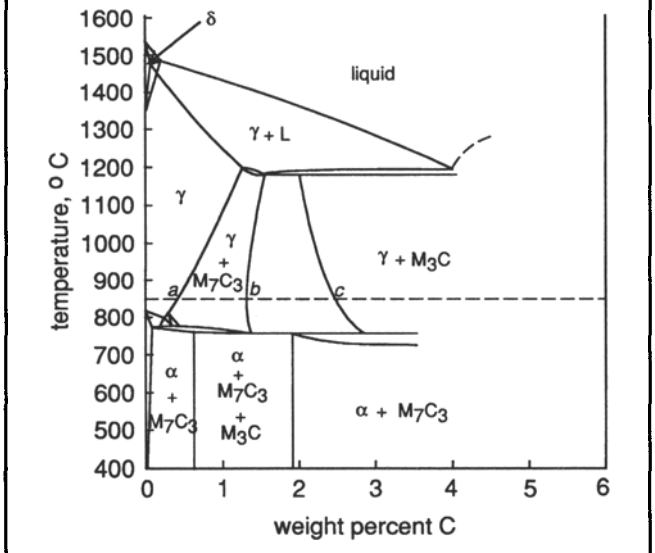

Fig. 18a Vertical section of the Fe-Cr-C phase diagram containing 5 wt.% Cr.

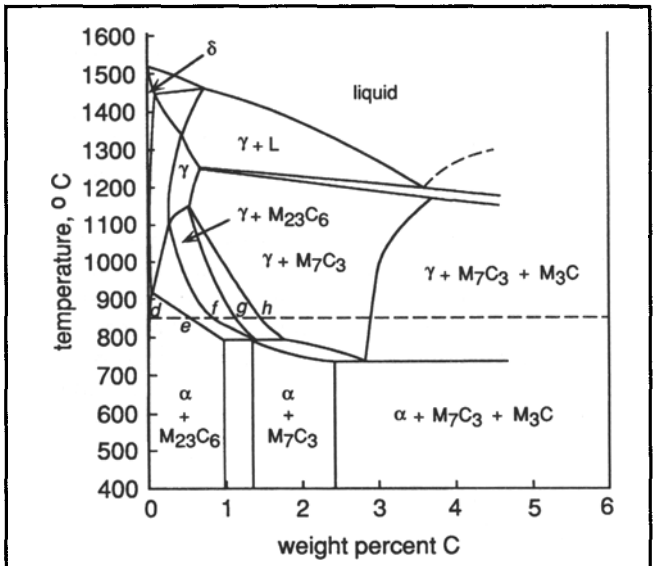

Fig. 18b Vertical section of the Fe-Cr-C phase diagram containing 17 wt.% Cr.

Cr. Figure 17 shows that the addition of Cr to austenite significantly decreases the solubility of carbon and has a significant influence on the equilibrium carbide phases formed at higher carbon contents. Chromium can replace Fe in Fe_3C to form an M_3C phase containing up to 16 wt.% Cr (the point *m* in Fig. 17a), and Fe can replace Cr in Cr_7C_3 to form an M_7C_3 phase containing up to 38 wt.% Fe (the point *n* in Fig. 17a). Figures 18a and b are vertical sections of Fig. 16 at, respectively, constant concentrations of Cr of 5 and 17 wt.%, and in each figure a horizontal broken line is drawn at 850 °C. Figure 17b shows that the replacement of iron by carbon in an alloy containing 5 wt.% Cr alloy causes saturation of the austenite at *a* at which point a carbide M_7C_3 is precipitated. Further replacement moves the system through the two-phase field with a decrease in the chromium content and an increase in the carbon content of the austenite, a decrease in the chromium content of the carbide phase, and an increase in the ratio of carbide to austenite. At *b*, the system enters the three-phase field of austenite with M_7C_3 of composition *n* in Fig. 17a and M_3C of composition *m*. Further replacement of iron by carbon decreases the relative amount of austenite occurring and causes the transformation of M_7C_3 of composition *n* to M_3C of composition *m*. This transformation is complete when the gross composition reaches *c* at which point the system enters the two-phase field of austenite and M_3C. Further replacement again decreases the chromium content and increases the carbon content of the austenite and increases the ratio of carbide to austenite. When the overall carbon content reaches 6.65 wt.%, the austenite phase disappears, and the system exists as M_3C of molar composition $Fe_{2.86}Cr_{0.17}C$. The influence of temperature on the compositions *a*, *b*, and *c* is shown in Fig. 18a.

The phase equilibria occurring in an alloy containing 17 wt.% Cr are also shown in Fig. 17b, which shows that the replacement of Fe by C causes the system to move through the ferrite phase field to *d*, through a two-phase field between *d* and *e*, through the three-phase austenite-ferrite-$M_{23}C_6$ field between *e* and *f*, through another two-phase field between *f* and *g*, through a second three-phase field between *g* and *h*, and then

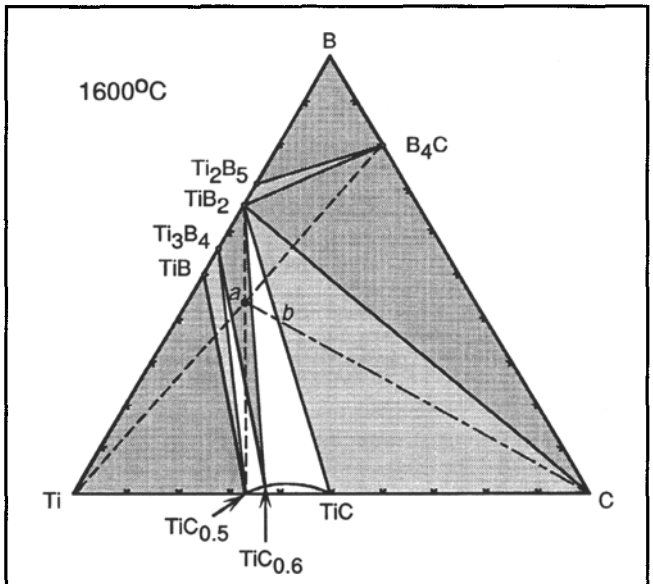

Fig. 19 Ti-B-C phase equilibrium at 1600 °C.

into a third two-phase field at *h*. The influence of temperature on the compositions *d*-*h* is shown in Fig. 18b.

The phase equilibria in the Ti-B-C system at 1600 °C, shown in Fig. 19, are of interest in the production of a composite material comprising hard titanium carbides in a titanium boride matrix. The isothermal section at 1600 °C contains: one single-phase field containing solid solutions ranging in composition from $TiC_{0.5}$ to TiC, 2 two-phase fields in which titanium carbide solid solutions are in equilibrium with Ti_3B_4 and with TiB_2, 4 quasibinary systems—$TiC_{0.5}$-TiB, TiB_2-C, TiB_2-B_4C, and Ti_2B_5-B_4C, and 7 three-phase fields. The phase diagram shows that, rather than the stoichiometric reaction

$$2Ti + \tfrac{1}{2}B_4C \rightarrow TiC_{0.5} + TiB_4 \quad \text{(Eq 1)}$$

occurring, the reaction of Ti and B_4C in the molar ratio 4:1 (the overall composition *a*) produces a three-phase mixture of Ti_3B_4, TiB_2, and $TiC_{0.6}$ according to:

$$4Ti + B_4C \rightarrow 0.333Ti_3B_4 + 1.333TiB_2 + 1.667TiC_{0.6} \quad \text{(Eq 2)}$$

Thus the hard carbide phase is produced in situ during the hot-pressing of a relatively plastic mixture of Ti and B_4C. Subsequent saturation of this composite with carbon causes the composition to move from *a* to *b*, which is a carbon-saturated composite of TiB_2 and the harder carbide TiC.

Stainless steels are Fe-Cr-based alloys, which under oxidizing conditions, form Cr_2O_3 as the protective product of oxidation, and consequently, the "stainless" quality of these alloys can be understood by consideration of phase equilibria in the Fe-Cr-O system. Figure 20a shows the phase equilibria in the Fe-Cr-O system presented on a Gibbs triangle at 1300 °C. Fe_2O_3 and Cr_2O_3 have the corundum crystal structure, and because of the similar radii of the Fe^{3+} and Cr^{3+} ions, the oxides form a complete series of solid solutions. Also the spinels $FeO.Fe_2O_3$ and $FeO.Cr_2O_3$ form a complete series of solid solutions. The system Fe-O also contains wustite, which is a range of solid solutions that occur at O/Fe ratios greater than unity. The isothermal section shown in Fig. 20a also contains 3 three-phase fields and 5 two-phase fields. Figure 20b shows the phase equilibria in the subsystem FeO-Fe_2O_3-Cr_2O_3,[5] and Fig. 20c shows the phase equilibria in the Fe-Cr-O system using the ratios $X_O/(X_{Fe} + X_{Cr})$ and $X_{Cr}/(X_{Cr} + X_{Fe})$ as cartesian coordinates. In each of Fig. 20a-c, the tie-lines in the two-phase fields are also oxygen isobars.

Phase equilibria in a system in which one of the components is a reactive gas, such as oxygen, are best displayed in a phase stability diagram, in which the phase and reaction equilibria are shown as functions of the pressure of the reactive gas. From the phase rule, in a ternary system that includes a gaseous phase, the maximum number of condensed phases that can coexist at an arbitrary temperature is three. The phase stability diagram for the Fe-Cr-O system is shown in Fig. 20d. Consider the equilibrium behavior of an Fe-Cr alloy of $X_{Cr} = 0.7$ subjected to a gaseous atmosphere in which the pressure of oxygen is continuously increased from a starting value of 10^{-18} atm. The α phase is stable until the pressure of oxygen reaches $10^{-15.2}$ (the point *a* in Fig. 20d), in which state Cr_2O_3 is formed as an oxidation product. In practice, the formation of this protective film of Cr_2O_3 virtually isolates the metallic alloy from the gas phase and, hence, renders the alloy stainless. However, considering that thermodynamic equilibrium is established, further increase in the pressure of oxygen moves the system into the two-phase field in which the composition of the α moves along the phase boundary line towards *b*, and the relative amounts of α and Cr_2O_3 phases are given by the lever rule applied to the tie-line between the compositions of the two equilibrated phases. At $p_{O_2} = 10^{-14.4}$ atm (point *c*), the three-phase equilibrium α-γ-Cr_2O_3 occurs, and further increase in the pressure of oxygen moves the system into the two-phase γ-Cr_2O_3 field in which the composition of the γ phase moves along the phase boundary from *b* towards *d*. The three-phase equilibrium γ-spinel-Cr_2O_3 occurs at $p_{O_2} = 10^{-13.4}$ atm (the point *e*). Further increase in the oxygen pressure moves the system through the two-phase γ-spinel field between *e* and *g*, gives a three-phase equilibrium at *g*, moves the system through the wustite-spinel field between *g* and *i*, through the single-phase spinel field between *i* and *j*, through the two-phase field between *j* and *k*, and finally into the single-phase sesquioxide field at oxygen pressures greater than $10^{-2.7}$, the point *k*.

Figure 20d shows that formation of the protective oxide Cr_2O_3 at 1300 °C on the metallic alloy requires that the mole fraction of Cr be at least 0.02 (the point *d*). Alloys containing less Cr oxidize along the line *d*-*f* to form a nonprotective spinel scale or along the line *f*-*h* to form a nonprotective wustite scale.

Another form of phase stability diagram is shown in Fig. 21a and b, which are drawn for the Si-C-O system at 1000 °C. In this case, the reactive gas phase is a mixture of CO and CO_2, and again, the maximum number of condensed phases that coexist at an arbitrary temperature is three. In a ternary system, fixing the thermodynamic activities of two of the components fixes the activity of the third component and, hence, fixes the state of existence of the system. Thus in Fig. 21a, the phase equilibria are shown as functions of the activity of carbon and

the activity of oxygen (which, for convenience, is taken to be the partial pressure of oxygen in the gas phase). The stability diagram contains fields of stability of Si, SiC, and SiO_2, which meet at lines along which two condensed phases are in equilibrium with the gas phase, and the three lines meet at the unique values of the activities of carbon and oxygen at which the three condensed phases are in equilibrium with the gas phase at 1000 °C. Zero on the log a_C represents carbon existing at unit activity, and hence the upper bounds of the stability fields of SiC and SiO_2 represent saturation of these phases with carbon. The diagram also contains isobars for gaseous SiO. The boundary line between the fields of stability of SiC and Si is horizontal because the reaction equilibrium is independent of the pressure of oxygen, and the boundary line between the fields of stability of Si and SiO_2 is vertical because the reaction equilibrium is independent of the activity of carbon. The unit slope of the boundary line between the fields of stability of SiC and SiO_2 is determined by the stoichiometry in the equilibrium

$$SiO_2 + C = SiC + O_2$$

Fixing the values of the activity of carbon and the partial pressure of oxygen uniquely fixes the partial pressures of CO and CO_2 in the gas phase by means of the equilibria

$$C + \tfrac{1}{2}O_2 = CO$$

and

$$C + O_2 = CO_2$$

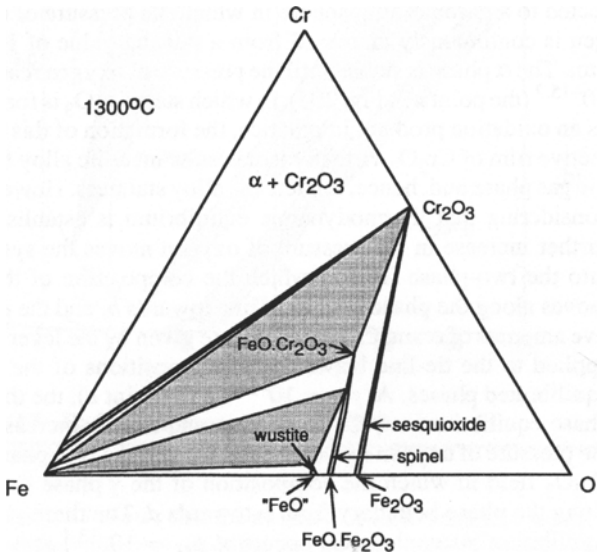

Fig. 20a Fe-Cr-O phase equilibrium at 1300 °C.

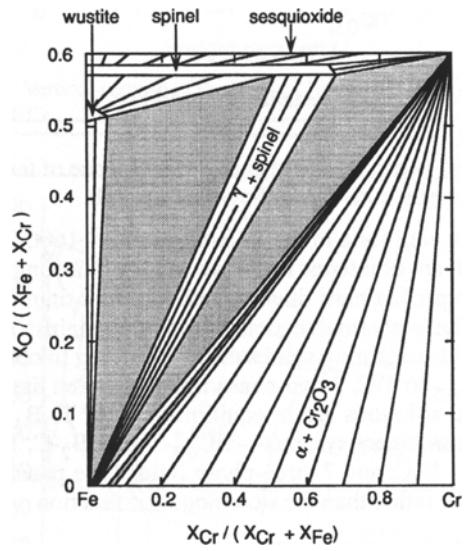

Fig. 20c Fe-Cr-O phase equilibrium at 1300 °C.

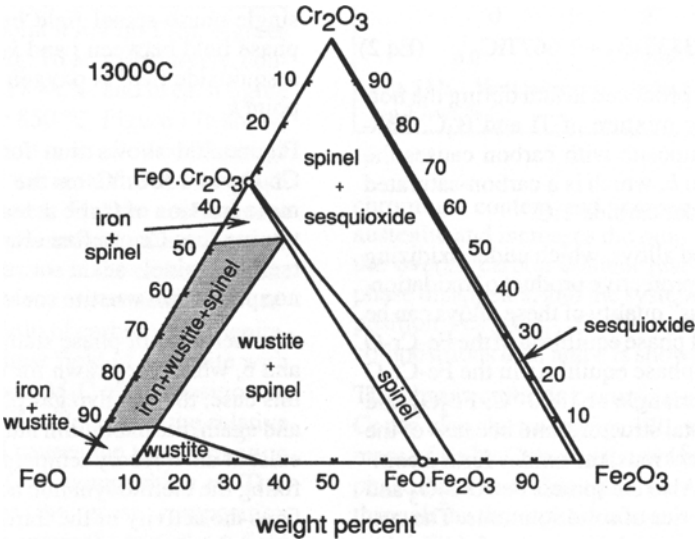

Fig. 20b FeO-Fe_2O_3-Cr_2O_3 phase equilibria at 1300 °C.

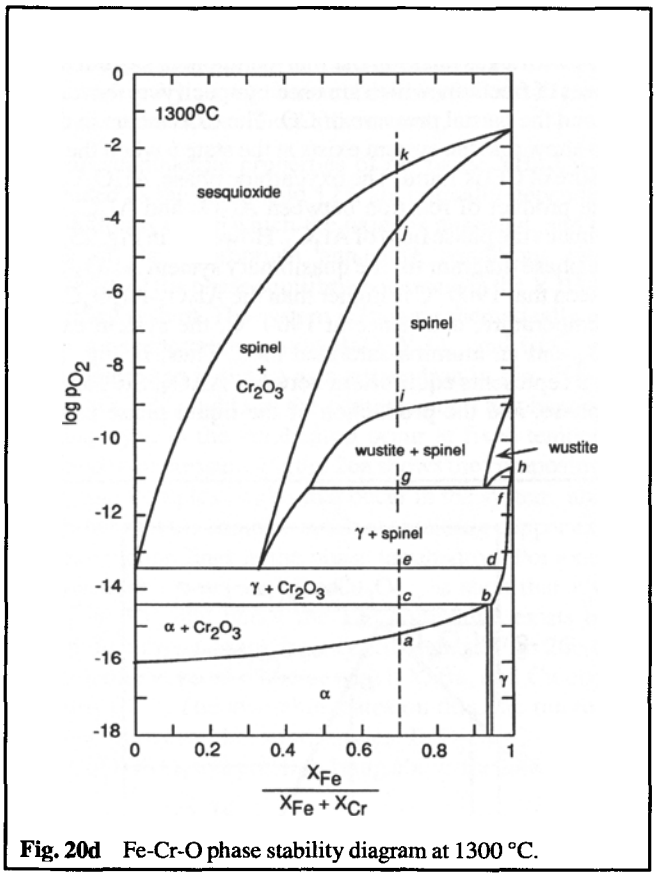

Fig. 20d Fe-Cr-O phase stability diagram at 1300 °C.

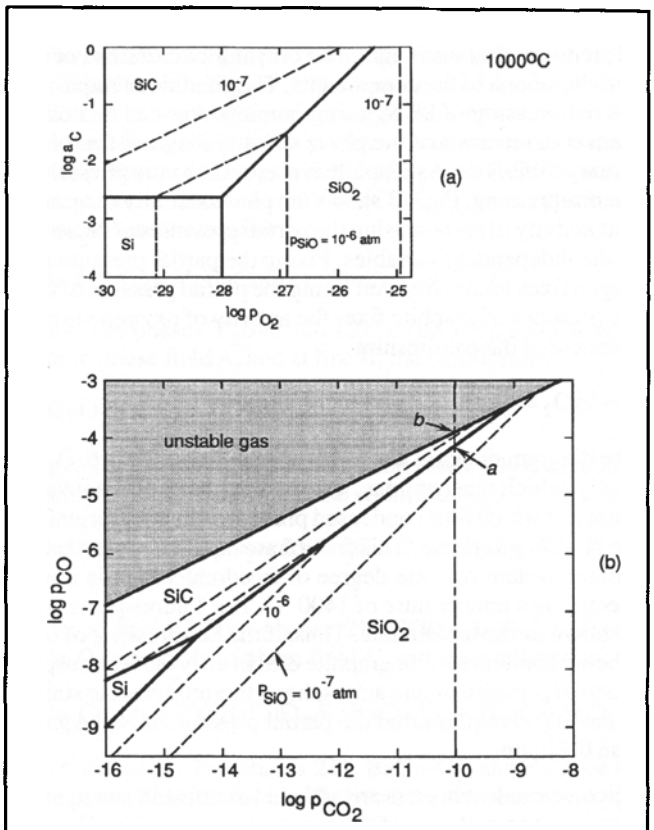

Fig. 21 Si-C-O phase stability diagram at 1000 °C.

and, hence, Fig. 21a can be redrawn as Fig. 21b using the partial pressures of CO and CO_2 as coordinates. The slopes of the phase boundary lines in Fig. 21b are determined by the stoichiometries in the equilibria

$$SiC + CO_2 = Si + 2CO$$

$$Si + 2CO_2 = SiO_2 + 2CO$$

and

$$SiC + 3CO_2 = SiO_2 + 4CO$$

The line between the field of stability of SiC and the region labeled "unstable gas" is the continuum of states in which carbon exists at unit activity. Thus, attempts to produce a CO-CO_2 gas mixture in the field of "unstable gas" cause the sooting-out of carbon from the gas according to

$$2CO_2 \rightarrow C + CO_2$$

until the composition of the gas has been changed to that which is in equilibrium with carbon at 1000 °C. The complete phase stability diagram for a ternary system is a three-dimensional diagram, and the influence of temperature on the phase equilibria in the Si-C-O system is shown in Fig. 22, which is the isobaric section of the three-dimensional diagram drawn for $p_{CO_2} = 10^{-10}$ atm. The states *a* and *b* in Fig. 21b correspond to the states *a* and *b* in Fig. 22. The stability diagram for the Si-C-O system gives the thermodynamic conditions necessary for the production of silicon carbide.

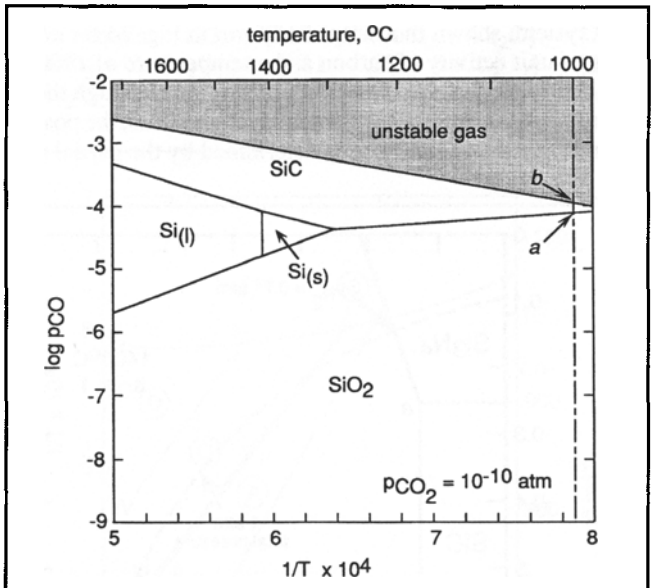

Fig. 22 Section of the Si-C-O phase stability diagram at $p_{CO_2} = 10^{-10}$ atm.

Quaternary Systems

Fixing the activities of three of the components of a quaternary system fixes the activity of the fourth component, and hence presentation of the phase equilibria in a quaternary system on

an isothermal phase stability diagram, such as shown in Fig. 21, requires that the diagram be drawn for conditions of fixed activity of one of the components. The conditions required for the hot pressing of Si_3N_4 using graphite dies can be obtained from consideration of the phase stability diagram for the quaternary Si-C-N-O. As graphite is present as a pure phase during the hot-pressing, Fig. 23 shows the phase stability diagram for unit activity of carbon using the partial pressures of N_2 and CO as the independent variables. Fixing the partial pressure of nitrogen fixes its activity, and fixing the partial pressure of CO in the presence of graphite fixes the activity of oxygen via establishment of the equilibrium

$$C + \tfrac{1}{2}O_2 = CO$$

The diagram contains the fields of stability of SiC, SiO_2, and Si_3N_4, which meet at lines, and the lines meet at the invariant point *a* at which four condensed phases are in equilibrium with the N_2-CO gas phase. This five-phase equilibrium in the quaternary system has one degree of freedom, which is used by specifying a temperature of 1400 °C. The 1 atmosphere isobar is shown as the broken line. Thus, if the hot-pressing of Si_3N_4 is being conducted with graphite dies in an N_2-CO atmosphere at a total pressure of one atmosphere, thermodynamic stability of the Si_3N_4 requires that the partial pressure of N_2 be greater than 0.71 atm.

Silicon carbide whiskers are added to alumina in an attempt to increase the toughness of the composite ceramic, and bonding between the two phases is facilitated by liquid-phase sintering. The conditions under which the required liquid phase is formed are given by the phase stability diagram for the Al-Si-C-O system, shown in a simplified form in Fig. 24 for conditions of unit activity of carbon and a temperature of 1900 °C. SiC and Al_2O_3 coexist along the *ac* line, and although the coordinates p_{Al_2O} and p_{SiO} are impractical variables, the position of the system on the *ac* line is determined by the partial pressure of CO in the gas phase. Coexistence of graphite, SiC, and Al_2O_3 with a gas phase in the four-component system has two degrees of freedom, which are used by specifying the temperature and the partial pressure of CO. The CO isobars in the diagram show that the system exists at the state *b* when the partial pressure of CO is 1 atm. The oxycarbide phase, Al_4O_4C, forms as the product of reaction between Al_2O_3 and Al_4C_3, and it eliminates the phase field of Al_4C_3. However, in Fig. 25, which is the phase diagram for the quasibinary system Al_2O_3-Al_4C_3, it is seen that 1900 °C is higher than the Al_2O_3-Al_4O_4C eutectic temperature, and hence at 1900 °C, the system exists as Al_2O_3 and an alumina-saturated melt. Thus, in Fig. 24, the state *a* represents equilibrium between Al_2O_3, SiC, and a liquid phase, and the production of the liquid phase facilitates

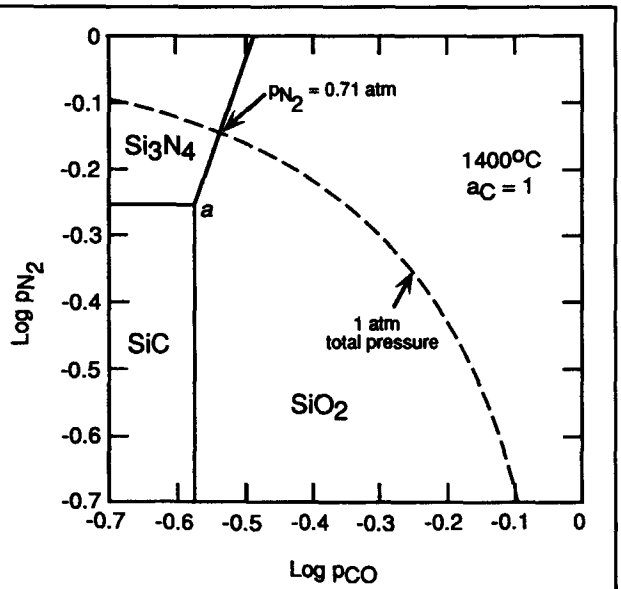

Fig. 23 Si-C-N-O stability diagram at 1400 °C and unit activity of carbon.

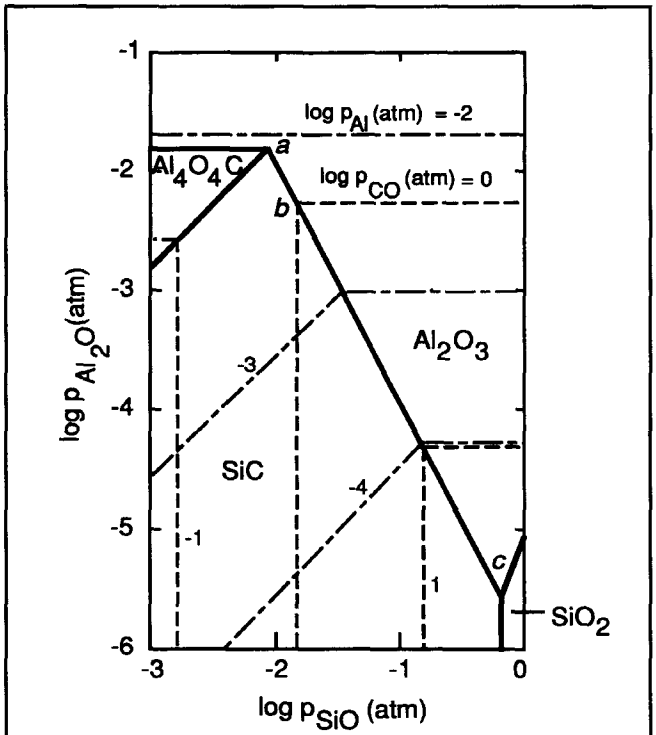

Fig. 24 Al-Si-C-O stability diagram at 1900 °C and unit activity of carbon.

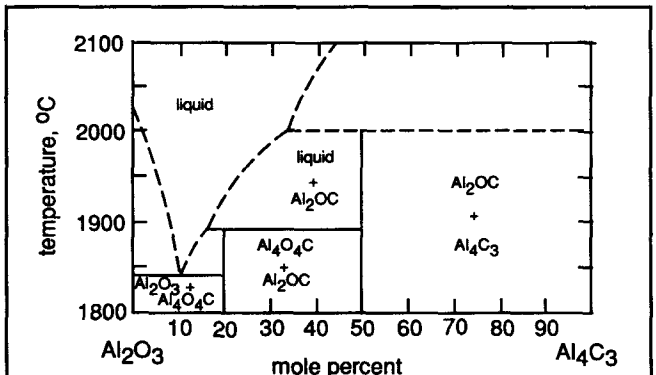

Fig. 25 Quasibinary Al_2O_3-Al_4C_3 phase diagram.

densification during sintering. The state *a* is attained by maintaining the partial pressure of CO at 0.55 atm. At 1900 °C, the state *c* is actually an equilibrium between SiC, Al_2O_3, and an alumina-saturated aluminum silicate melt.

The superconducting properties of the oxide $YBa_2Cu_3O_{7-x}$, designated as the compound 123, are critically dependent on the conditions under which the oxide is annealed, and hence choice of the appropriate annealing conditions requires knowledge of the phase equilibria occurring in the Y-Ba-Cu-O quaternary system. The system is shown schematically in Fig. 26a as a pseudoternary using BaO, Y_2O_3, and CuO_x as the components, and is shown as a tetrahedron in Fig. 26b using BaO, Y_2O_3, Cu, and O as the components. The phase equilibria displayed in the tetrahedron occur at fixed temperature and fixed total pressure. Figure 26a shows the compositions of the various complex oxides that occur in the system, and Fig. 26b shows that the complex oxides containing copper exist on oxygen reaction lines in the phase tetrahedron. For example, the nonstoichiometry in $YBa_2Cu_3O_{7-x}$ is such that x varies from 0 to 1.0, and hence the 123 compound exists on the straight line drawn from the oxygen apex in Fig. 26b to the position on the basal plane at which Y, Ba, and Cu occur in the ratio 1:2:3. The available states on this line range from midway between the subtriangles BaO-Cu_2O-Y_2O_3 and BaO-CuO-Y_2O_3 to a position lying above the latter triangle,

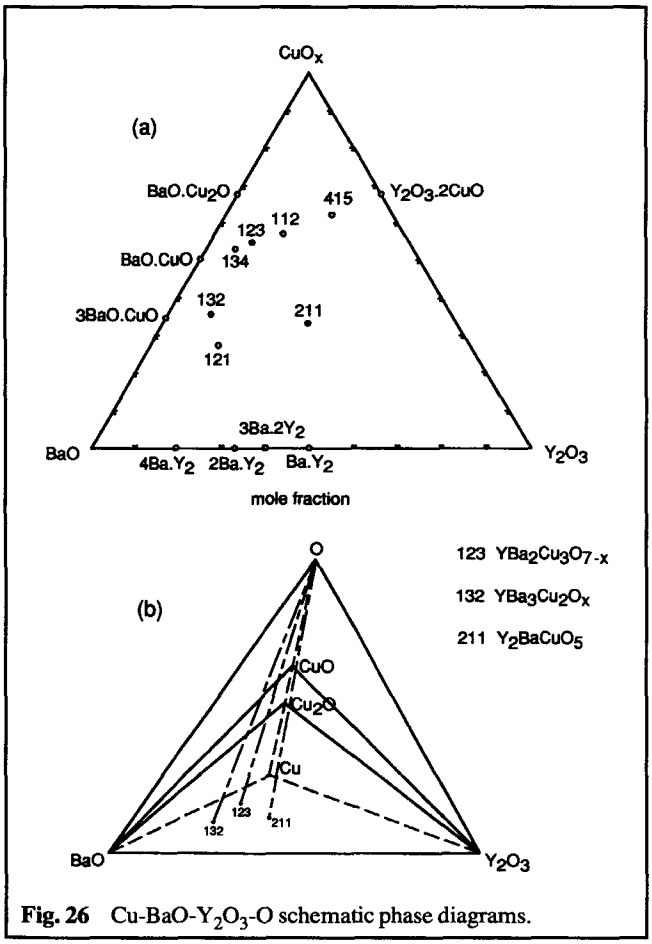

Fig. 26 Cu-BaO-Y_2O_3-O schematic phase diagrams.

with the actual state of existence being determined by the temperature and the oxygen pressure. The phase stability diagram for 123 is shown in Fig. 27.[6] The sequence of decomposition of 123 can be seen by considering an isothermal line in Fig. 27 along which the oxygen pressure is decreased. Decreasing the pressure of oxygen in the 123 phase field causes an increase in the value of x in $YBa_2Cu_3O_{7-x}$ to unity at line I, in which state the equilibrium

$$2YBa_2Cu_3O_6 = Y_2BaCuO_5 + 3BaCuO_2 + Cu_2O$$

occurs. The phases Y_2BaCuO_5 (211), $BaCuO_2$, and Cu_2O are stable in phase field *A*, and at line II, the equilibrium

$$2BaCuO_2 + Cu_2O = 2BaCu_2O_2 + \tfrac{1}{2}O_2$$

occurs. The phases 211, $BaCuO_2$, and $BaCu_2O_2$ are stable in the narrow phase field *B*, and the equilibrium

$$Y_2BaCuO_5 + 7BaCuO_2 = 2YBa_3Cu_2O_6 + 2BaCu_2O_2 + 1.5O_2$$

occurs at line III. The phases 211, $YBa_3Cu_2O_6$ (132), and $BaCu_2O_2$ are stable in phase field *C*, and the equilibrium

$$4YBa_3Cu_2O_6 = 2Y_2BaCuO_5 + 3BaCu_2O_2 + 7BaO + \tfrac{1}{2}O_2$$

occurs at line IV. The phases 211, $BaCu_2O_2$, and BaO are stable in phase field *D*, and line V shows the influence of oxygen pressure on the temperature at which incongruent melting occurs. Thus decreasing the partial pressure of oxygen at constant temperature or increasing the temperature at constant partial pressure of oxygen causes 123 to decompose according to the sequence 123 → [211 + $BaCuO_2$ + Cu_2O] → [211 + $BaCuO_2$ + $BaCu_2O_2$] → [211 + 132 + $BaCu_2O_2$] → [211 + $BaCu_2O_2$ + BaO], and the phase stability diagram shows that

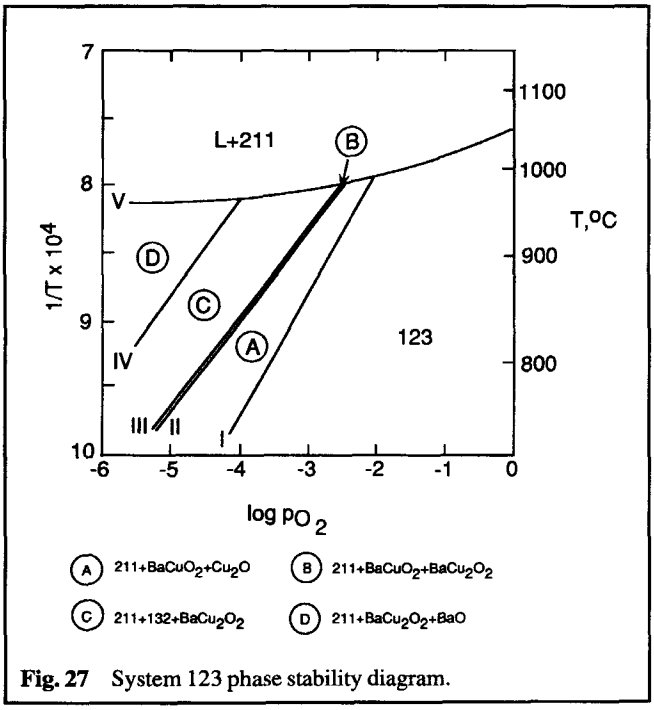

Fig. 27 System 123 phase stability diagram.

the compound 123 must be annealed under conditions that lie to the right of line I.

Cited References

1. A.D. Pelton, *Physical Metallurgy,* 3rd ed., Part 1, R.W. Cahn and P. Haasen, Ed., North Holland Physics Publishing, New York, NY, 356 (1983).
2. Y.A. Chang, J.P. Neumann, and U.V. Choudary, *Phase Diagrams and Thermodynamic Properties of Ternary Copper-Sulfur-Metal Systems,* INCRA Monograph Series VII, New York, NY, 136 (1979).
3. M. Uredricek and J.S. Kirkaldy, *Z. Metallkd., 64,* 899 (1973).
4. C.R. Brookes, *Heat Treatment of Ferrous Alloys,* McGraw-Hill Publishing Co., New York, 149 (1979).
5. T. Katsura and A. Muan, *Trans. AIME, 230,* 80 (1964).
6. J.S. Kim, Ph. D. thesis, Purdue University (1992).